DOI: 10.31401/WS.2025.proc.06

Nonlinear and Causal Dynamics between Solar and Geomagnetic Activity Indices: Findings from Chaos and Causality Measures

Kilcik A., Gerçeker K.

Department of Space Sciences and Technologies, Akdeniz University Faculty of Science, 07058, Antalya, Türkiye.
alikilcik@akdeniz.edu.tr, kemalhangerceker@gmail.com

Abstract

This study aims to identify nonlinear/chaotic features and causal relationships among monthly SSN, F10.7, aa, and Dst indices over December 1963–March 2025. Phase-space is reconstructed via AMI-selected delay τ and FNN dimension E; we estimate the Hurst exponent H, the largest Lyapunov exponent λ, and the correlation dimension D_2; and apply CCM with SSN as reference. H spans $0.84 - 0.93$ ($SSN \approx 0.93$; $F10.7 \approx 0.93$; $aa \approx 0.88$; $Dst \approx 0.84$), indicating strong persistence. λ ranges from ≈ 0.010 to ≈ 0.040 (highest for Dst, lowest for aa), implying deterministic chaos with finite prediction horizons. D_2 varies between $3.37 - 3.86$, consistent with low–moderate dimensional structure. CCM analysis shows a strong linear relationship between SSN–F10.7, while indicating a non-linear causal relationship between SSN and other indices. In conclusion, sunspot variability affects global geomagnetic activity continuously and nonlinearly on a monthly scale; this effect is most pronounced for aa and weaker for Dst.

Keywords: Chaos; Nonlinear and Causality Analyses; Solar and Geomagnetic Activity

1. Introduction

Understanding how solar activity and geomagnetic variability co-evolve is essential for space weather predictions and its impacts on satellites, navigation and communication, aviation, etc., (Eastwood et al., 2017). At geospace scales, energy transfer is controlled by solar-wind/IMF coupling; sustained southward IMF and strong convection electric fields build the ring current and trigger geomagnetic storms (Dungey 1961; Echer et al., 2008).

Here, we analyzed monthly indices that together sample the driver and the response: the international sunspot number (SSN), the 10.7 cm solar radio flux (F10.7), the geomagnetic aa index, and the disturbance storm-time (Dst) index. SSN and F10.7 are tracers of solar magnetic activity and EUV variability (Hathaway 2015; Tapping 2013). The aa index provides a long-term global geomagnetic activity (Mayaud, 1972), while Dst tracks the storm-time low-latitude magnetic depression in short time primarily due to the ring current and is widely used as a standard storm metric (Gonzalez et al., 1994). Taken together, these series allow for a joint view of memory, nonlinearity, and possible Sun-geospace directionality on monthly scales.

We reconstruct dynamics with delay coordinates, choosing the time delay τ by Average Mutual Information and the embedding dimension E by False Nearest Neighbors (Fraser & Swinney 1986; Kennel et al., 1992). In these embeddings we estimate the Hurst exponent H for persistence (Hurst 1951), the largest Lyapunov exponent λ for sensitivity and prediction limits (Rosenstein et al., 1993),, and the correlation dimension D_2 for effective dimensionality (Grassberger & Procaccia 1983a). To go beyond correlation, we use Convergent Cross Mapping to test for directional/causality influence via library-size convergence and asymmetry of cross-map skill (Sugihara et al., 2012).

There is an ongoing debate as to whether the variability of the solar cycle is primarily low-dimensional deterministic or largely stochastic. Evidence exists on both sides, but recent reviews and data-driven models point to mixed dynamics and limited predictability horizons

(Petrovay 2020; Wang et al., 2025). In this study, we aim to quantify persistence and predictability, estimate dimensionality, and determine the directional connections between SSN, F10.7, aa, and Dst in order to establish a clear basis for future results.

2. Data and Methods

In this study, four indices were analyzed using monthly data for the time intervals December 1963—March 2025. The monthly sunspot number (SSN) was obtained from WDC—SILSO (Royal Observatory of Belgium, https://www.sidc.be/SILSO/). The 10.7 cm solar radio flux (F10.7, SFU) was obtained as daily values from NASA/OMNIWeb (https://omniweb.gsfc.nasa.gov/), and monthly averages were calculated. The Dst index (nT) was obtained as hourly values from the Geomagnetism WDC/Kyoto (https://wdc.kugi.kyoto-u.ac.jp/dstdir/), and monthly averages were calculated. The aa index (nT) was obtained as 3-hourly values from the International Service of Geomagnetic Indices (ISGI, https://isgi.unistra.fr/indices_aa.php) and similarly converted to monthly averages. All subsequent analyses were performed on these monthly series within the above time period.

For nonlinear analyses, each scalar series $x(t)$ was embedded via delay coordinates

$$X(t) = [x(t), x(t-\tau), \dots, x(t-(E-1)\tau)], \tag{1}$$

with delay τ chosen as the first local minimum of Average Mutual Information (AMI) (Fraser & Swinney 1986) and embedding dimension E by False Nearest Neighbors (FNN) (Kennel et al., 1992), following the embedding theorem of Takens' (Takens 1981). A Theiler window (Theiler 1986) was applied when selecting the nearest neighbors to suppress temporal autocorrelation effects. Also, the long-memory (persistence) of the data is estimated by using Hurst exponent (H) analysis. This analysis follows the standard convention: $H > 0.5$ persistent, $H = 0.5$ memory-less random walk, $H < 0.5$ anti-persistent (Hurst 1951; Mandelbrot & Wallis 1969). Sensitivity to initial conditions and practical predictability limits are quantified by calculating the largest Lyapunov exponent (λ). The largest Lyapunov exponent: $\lambda > 0$ indicates deterministic chaos, $\lambda \approx 0$ neutrality/periodicity, and $\lambda < 0$ convergence (Rosenstein et al., 1993). To calculate the predictability of the data set used the correlation dimension (D_2) analysis (Grassberger & Procaccia 1983a,b). Finally, to test directionality beyond co-variation, we used Convergent Cross Mapping CCM (Sugihara et al., 2012).

The chosen methods provide complementary views of the monthly SSN, F10.7, aa, and Dst series. By using these methods together, it is possible to (i) quantify persistence and prediction limits, (ii) estimate effective dimensionality, and (iii) identify directional connections between the Sun and space. This provides a clear and repeatable basis for subsequent results.

3. Results

Here, we analyzed the monthly average SSN, F10.7, aa, and Dst indices for the period between January 1957 and March 2025.

(1) Hurst Exponent (H)

Figure 1 shows Hurst exponent analysis ($log(R/S)$ versus $log(n)$ with fitted slopes) for all data sets. The fitted slopes give $H(SSN) = 0.9255$, $H(F10.7) = 0.9324$, $H(aa) = 0.8835$ and $H(Dst) = 0.8446$. All H values are well above 0.5, which means the series are positively autocorrelated and display strong persistence: increases (decreases) tend to be followed by increases (decreases) at monthly scales rather than reverting quickly to the mean. So trend continuity is a common feature across the system in a monthly period. All proxies are very close in magnitude consistent with its smoother month-to-month evolution and the fact that all indices are shaped by the solar cycle and its sub-annual modulation. In practical terms, these H values indicate that low-frequency variability dominates the monthly signal; short runs of oppositesigned fluctuations do occur, but the longer-range tendency is to continue the prevailing trend.

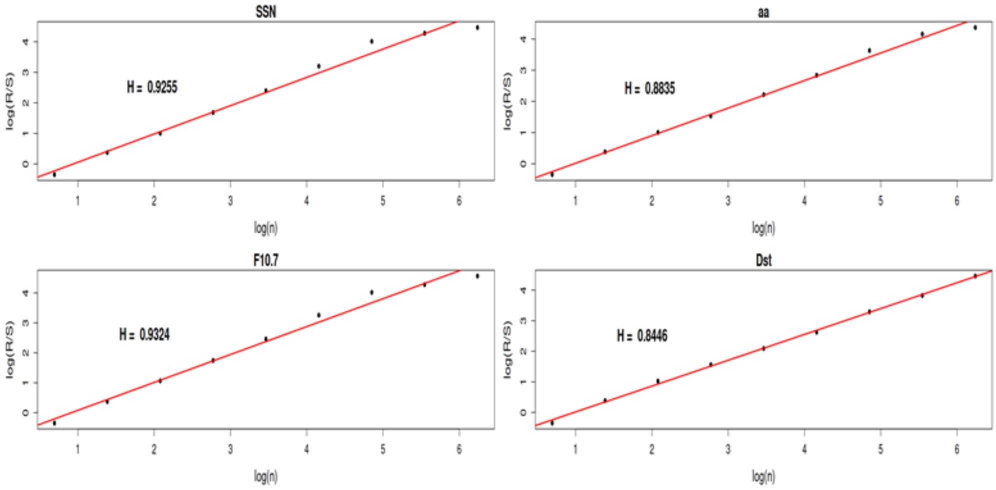

Figure 1. *Hurst exponent (H) analysis results for all data sets used in this study.*

(2) Largest Lyapunov Exponent (λ)

Figure 2 plots $S(t)$ versus evolution steps with the linear segment used to estimate the largest Lyapunov exponent for the used data sets. Linear segments of $S(t)$ yield $\lambda(SSN) = 0.02018$, $\lambda(F10.7) = 0.01433$. Since all are positive, the dynamics are chaotic in the deterministic sense and admit only a finite prediction horizon. The larger E means nearby trajectories diverge faster there than the smaller one, so short range predictions for data which has small λ decay a bit more quickly in skill. The gradual leveling of $S(t)$ at longer evolution steps is consistent with saturation once typical separations reach the attractor scale.

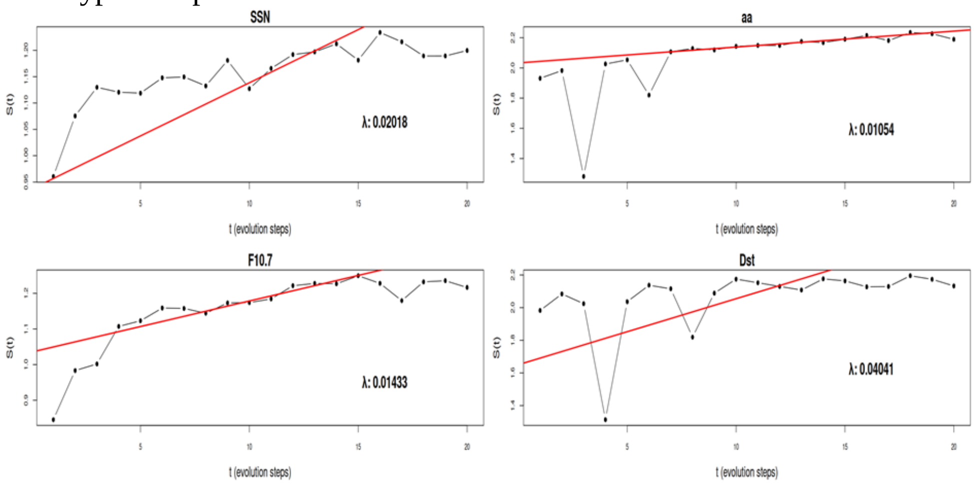

Figure 2. *Lyapunov exponent λ (growth of S(t)) and linear fits results for all data sets used in this study.*

The Dst value is the largest of the four, implying the shortest predictability window among these indices; conversely, aa has the smallest λ and thus the slowest divergence. In rank order of sensitivity to initial conditions we have $Dst > SSN > F10.7 > aa$. When combined with Hurst results, this means that the series can be both persistent and chaotic: trends continue on monthly scales, while fine-scale details can diverge quickly enough to limit deterministic predictions.

(3) Correlation Dimension (D_2)

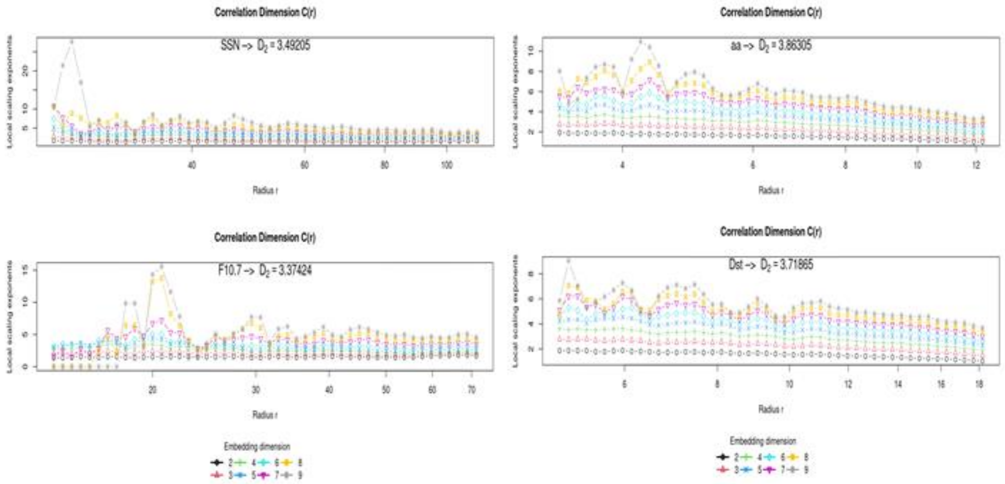

Figure 3. *Correlation Dimension D_2 (local scaling exponents and plateaus) results for the used data sets.*

Figure 3 displays local slopes of $logC(r)$ versus $logr$ and the plateau regions used to read off Correlation Dimension (D_2) for the used data sets. The plateau regions give $D_2(SSN) = 3.49205$, $D_2(F10.7) = 3.37424$, $D_2(aa) = 3.86305$ and $D_2(Dst) = 3.71865$. Dimensions in the $3-4$ range indicate low-to-moderate dimensional chaos: the dynamics are not purely random, but they also do not collapse to a near-periodic low-D structure. The closeness of the two values suggests that, despite different measurement bases, SSN and F10.7 share a similar effective number of active degrees of freedom on monthly scales.

(4) Convergent Cross Mapping (CCM)

Figure 7 plots cross-map skill $\rho(L)$ against library size L for each pair, with the dashed line showing the Pearson correlation. For SSN–F10.7, both directions rise and nearly coincide and they stay close to—but below—the Pearson correlation level (≈ 0.98). This points to very strong co-variation (linear relationship) dominated by the solar cycle, without a clear one-way driver at the monthly scale.

For SSN–aa, both curves increase with L and are above the Pearson correlation ($\rho \approx 0.41$), indicating nonlinear information beyond simple correlation. The curve that reconstructs SSN from aa is consistently higher and saturates (≈ 0.67) than the reverse reconstruct aa from SSN curve (≈ 0.57). By the CCM rule, this asymmetry supports the causal effect of SSN on aa (SSN → aa).

For SSN–Dst, both directions show a modest rise above the Pearson correlation level ($\rho \approx 0.38$). The reconstruct SSN from Dst curve is only slightly higher (≈ 0.454) than the reconstruct Dst from SSN curve (≈ 0.447), implying a weak SSN → Dst effect. Overall, CCM highlights clear SSN → aa causal relationship, weaker SSN → Dst causal relationship, and mainly linear relationship for SSN–F10.7.

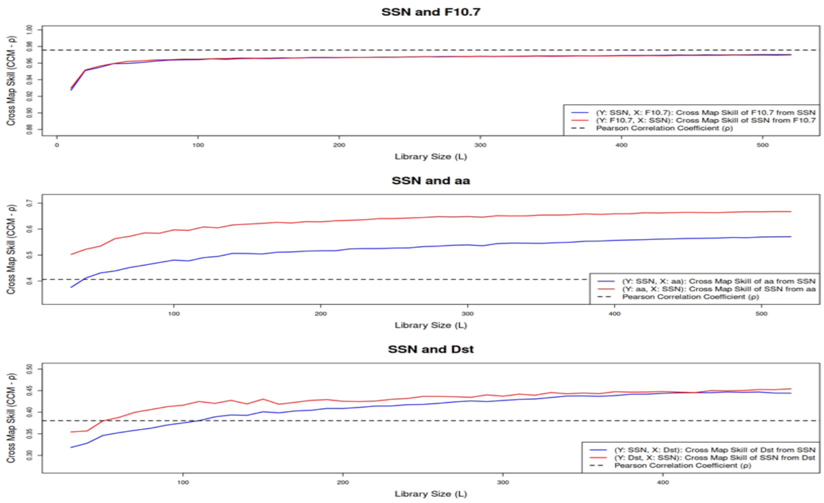

Figure 4. *Convergent Cross Mapping (Cross-map skill CCM-ρ(L) versus library size) results for the pairs SSN–F10.7, SSN–aa, and SSN–Dst (directions shown blue and red = CCM-ρ; black dashed line = Pearson ρ).*

4. Conclusion and Discussion

In this study, we analyzed monthly SSN, F10.7, aa, and Dst over January 1957–March 2025 using Hurst exponent (R/S), largest Lyapunov exponent, correlation dimension, and Convergent Cross Mapping (CCM). The findings of the study are as follows:

1. All indices have $H > 0.8$ ($SSN \approx 0.93$, $F10.7 \approx 0.93$, $aa \approx 0.88$, $Dst \approx 0.84$), indicating positive autocorrelation and trend continuity on monthly scales. The ordering $F10.7 \geq SSN > aa > Dst$ suggests that memory gradually weakens from solar to geomagnetic proxies.
2. The largest Lyapunov exponents (λ) are positive ($SSN \approx 0.020$, $F10.7 \approx 0.014$, $aa \approx 0.011$, $Dst \approx 0.040$). The sensitivity ranking $Dst > SSN > F10.7 > aa$ implies the shortest relative predictability for Dst and the longest for aa.
3. Correlation dimensions vary between $D_2 \approx 3\text{–}4$ ($SSN \approx 3.49$, $F10.7 \approx 3.37$, $aa \approx 3.86$, $Dst \approx 3.72$), consistent with low-to-moderate dimensional chaotic structure rather than pure randomness.
4. SSN–F10.7 shows a strong linear co-variation/relationship; SSN → aa and SSN → Dst indicate nonlinear causal relationships beyond simple correlation, with a clear driver role for SSN on aa and a weaker influence on Dst.

Our persistence results are consistent with the dominance of low-frequency variability linked to the solar cycle (Hathaway 2015) and with the long-memory behavior captured by R/S analysis (Hurst 1951; Mandelbrot & Wallis, 1969). Positive Lyapunov exponents indicate deterministic chaos and finite prediction horizons from the data themselves (Rosenstein et al., 1993). $D_2 \sim 3\text{–}4$ indicate a low-to-medium dimensional structure; this is not a completely random process, nor is it a system with a very low D_2 value that is nearly periodic (Grassberger & Procaccia, 1983a,b). These patterns align with current debates: while recent analyses have reported traces of low-dimensional dynamics in sunspot numbers, state-of-the-art investigations and dynamo modeling argue that the cycle behaves as a weak nonlinear, noise-perturbed limit cycle and is characterized by a mixture of deterministic-stochastic dynamics and inherently limited predictability (Cameron & Schüssler 2017, 2019; Petrovay 2020; Usoskin 2023; Huang

2025); observation-based iterative maps likewise indicate short cycle-to-cycle memory and prominent stochasticity (Wang et al., 2025).

The CCM results align with known physics of Sun–geospace relationship. The near-symmetric SSN–F10.7 curves reflect a common solar driver rather than a simple one-way causal chain. In contrast, SSN → aa is plausible because aa integrates global activity driven by solar-wind–magnetosphere coupling (Dungey 1961), and our asymmetric, saturating cross-map skills indicate information flow beyond static correlation (Sugihara et al., 2012). The weak SSN → Dst result is also reasonable: Dst strongly depends on the sustained southward IMF and enhanced convection (Gonzalez et al., 1994; Echer et al., 2008), that is, event-like conditions that monthly averaging can mute, reducing apparent directionality.

Acknowledgements

This study was supported by Project 124N011 awarded by the Scientific and Technological Research Council of Türkiye (TÜBİTAK). This study is also part of the Master of Science thesis of Kemalhan Gerçeker.

References

Cameron, R.H., Schüssler, M. (2017). Understanding solar cycle variability, *Astrophysical Journal*, Vol. 843, No. 2, 111, DOI: 10.3847/1538-4357/aa767a.

Cameron, R.H., Schuessler, M. (2019). Solar activity: Periodicities beyond 11 years are consistent with random forcing, *Astronomy and Astrophysics*, Vol. 625, A28, DOI: 10.1051/0004-6361/201935290.

Dungey, J.W. (1961). Interplanetary magnetic field and the auroral zones, *Physical Review Letters*, Vol. 6, No. 2, 47, DOI: 10.1103/PhysRevLett.6.47.

Eastwood, J.P., Biffis, E., Hapgood, M.A., Green, L., Bisi, M.M., Bentley, R.D., Burnett, C. (2017). The economic impact of space weather: Where do we stand?, *Risk Analysis*, Vol. 37, No. 2, pp. 206–218.

Echer, E., Gonzalez, W.D., Tsurutani, B.T., Gonzalez, A.C. (2008). Interplanetary conditions causing intense geomagnetic storms (Dst ≤ −100 nT) during solar cycle 23 (1996–2006), *Journal of Geophysical Research: Space Physics*, Vol. 113, A5, DOI: 10.1029/2007JA012744.

Fraser, A.M., Swinney, H.L. (1986). Independent coordinates for strange attractors from mutual information, *Physical Review A*, Vol. 33, No. 2, 1134, DOI: 10.1103/PhysRevA.33.1134.

Gonzalez, W.D., Joselyn, J.A., Kamide, Y., Kroehl, H.W., Rostoker, G., Tsurutani, B.T., Vasyliunas, V.M. (1994). What is a geomagnetic storm?, *Journal of Geophysical Research: Space Physics*, Vol. 99, No. A4, pp. 5771–5792, DOI: 10.1029/93JA02867.

Grassberger, P., Procaccia, I. (1983a). Characterization of strange attractors, *Physical Review Letters*, Vol. 50, No. 5, 346, DOI: 10.1103/PhysRevLett.50.346.

Grassberger, P., Procaccia, I. (1983b). Measuring the strangeness of strange attractors, *Physica D: Nonlinear Phenomena*, Vol. 9, No. 1–2, pp. 189–208, DOI: 10.1016/0167-2789(83)90298-1.

Hathaway, D.H. (2015). The solar cycle, *Living Reviews in Solar Physics*, Vol. 12, No. 1, 4, DOI: 10.1007/lrsp-2015-4.

Huang, L., Li, Q. (2025). Dynamical analysis of long-term solar activity based on ensemble empirical mode decomposition, *Monthly Notices of the Royal Astronomical Society*, Vol. 542, No. 1, pp. 136–150, DOI: 10.1093/mnras/staf1135.

Hurst, H.E. (1951). Long-term storage capacity of reservoirs, *Transactions of the American Society of Civil Engineers*, Vol. 116, No. 1, pp. 770–799, DOI: 10.1061/TACEAT.0006518.

Kennel, M.B., Brown, R., Abarbanel, H.D. (1992). Determining embedding dimension for phase-space reconstruction using a geometrical construction, *Physical Review A*, Vol. 45, No. 6, 3403, DOI: 10.1103/PhysRevA.45.3403.

Mandelbrot, B.B., Wallis, J.R. (1969). Robustness of the rescaled range R/S in the measurement of noncyclic long-run statistical dependence, *Water Resources Research*, Vol. 5, No. 5, pp. 967–988, DOI: 10.1029/WR005i005p00967.

Mayaud, P.N. (1972). The aa indices: A 100-year series characterizing the magnetic activity, *Journal of Geophysical Research*, Vol. 77, No. 34, pp. 6870–6874, DOI: 10.1029/JA077i034p06870.

Petrovay, K. (2020). Solar cycle prediction, *Living Reviews in Solar Physics*, Vol. 17, No. 1, 2, DOI: 10.1007/s41116-020-0022-z.

Rosenstein, M.T., Collins, J.J., De Luca, C.J. (1993). A practical method for calculating largest Lyapunov exponents from small data sets, *Physica D: Nonlinear Phenomena*, Vol. 65, No. 1–2, pp. 117–134, DOI: 10.1016/0167-2789(93)90009-P.

Sugihara, G., May, R., Ye, H., Hsieh, C.-H., Deyle, E., Fogarty, M., Munch, S. (2012). Detecting causality in complex ecosystems, *Science*, Vol. 338, No. 6106, pp. 496–500, DOI: 10.1126/science.1227079.

Takens, F. (1981). Detecting strange attractors in turbulence, in: Rand, D., Young, L.-S. (eds), *Dynamical Systems and Turbulence, Warwick 1980*, *Lecture Notes in Mathematics*, Vol. 898, Springer, Berlin, Heidelberg, DOI: 10.1007/BFb0091924.

Tapping, K.F. (2013). The 10.7 cm solar radio flux (F10.7), *Space Weather*, Vol. 11, No. 7, pp. 394–406, DOI: 10.1002/swe.20064.

Theiler, J. (1986). Spurious dimension from correlation algorithms applied to limited time-series data, *Physical Review A*, Vol. 34, No. 3, 2427, DOI: 10.1103/PhysRevA.34.2427.

Usoskin, I.G. (2023). A history of solar activity over millennia, *Living Reviews in Solar Physics*, Vol. 20, No. 1, 2, DOI: 10.1007/s41116-023-00036-z.

Wang, Z.F., Jiang, J., Wang, J.X. (2025). Observation-based iterative map for solar cycles. I. Nature of solar cycle variability, *Astrophysical Journal*, Vol. 984, No. 2, 183, DOI: 10.3847/1538-4357/adc72d.